Nigerian Journal of Technology (NIJOTECH)
Vol. 44, No. 3, September, 2025, pp.401- 410
www.nijotech.com

Print ISSN: 0331-8443
Electronic ISSN: 2467-8821
https://doi.org/10.4314/njt.v44i3.4

SOL-GEL SYNTHESIS AND ADVANCED CHARACTERISATION OF TITANIUM DIOXIDE NANOPARTICLES

AUTHORS:
W. C. Ulakpa[1,*], O. S. Azeez[2], and M. A. Olutoye[3]

AFFILIATIONS:
[1,2,3]Department of Chemical Engineering, Faculty of Engineering, Federal University of Technology, Minna, Nigeria.
[1]Department of Chemical Engineering, Faculty of Engineering, Southern Delta University, Ozoro, Nigeria.

***CORRESPONDING AUTHOR:**
Email: ulakpa.wisdom@yahoo.com

ARTICLE HISTORY:
Received: 19 December, 2024.
Revised: 27 June, 2025.
Accepted: 06 July, 2025.
Published: October 15, 2025.

KEYWORDS:
Sol-gel Synthesis, Calcination, Nanoparticles, Titanium dioxide, Anatase, Characterization.

ARTICLE INCLUDES:
Peer review

DATA AVAILABILITY:
On request from author(s)

EDITORS:
Ozoemena Anthony Ani

FUNDING:
None

Abstract

The sol-gel method was used in this study to synthesis Titanium Dioxide (TiO2) Nanoparticles (NPs) using Titanium (iv) isopropoxide as precursor material. Thereafter, the resultant xerogel was calcined at 400 ^{O}C. The synthesized nanoparticles were dried at 100ºC for 2 hours and calcined at 400ºC for 3 hours. The particles were characterized by Thermogravimetric analysis/differential scanning calorimetry (TGA/DSC), high-resolution transmission electron microscopy (HRTEM), Brunauer-Emmett-Teller (BET/BJH) analysis, X-ray diffraction (XRD), X-ray fluorescence (XRF), Field Emission Scanning Electron Microscopy (FESEM), Fourier-transform infrared spectroscopy (FTIR), and X-ray photoelectron spectroscopy (XPS). The nanoparticles revealed an anatase phase when heated to 400˚C, according to the X-ray diffraction (XRD) examination. Further analysis revealed a crystallite size of 11.71 nm and an average particle size of 24.48 nm for the nanoparticles. The investigation additionally showed that the nanoparticles exhibited 11.71 nm crystallites with particles sized of 24.48 nm on average. Spherical particles with a diameter of at least 50 nm were visible in TEM examinations. In agreement with TEM results, XRD data verified the particles' excellent purity and crystallinity. The BET/BJH result shows a mean pore width of 3.685 nm which indicate mesoporous structure, pore volume of 0.04367 cm3g, and surface area of 23.701 m^2/g. The Ti 2p orbital was found to exist in the oxidation states of +4 by X-ray photoelectron spectroscopy. This work focuses on the production of TiO_2 nanoparticles using a simple sol-gel synthesis technique and their thorough characterisation. The objective of this research is create titanium dioxide nanoparticles with better stability, reactivity, and performance than conventional methods and to promote the development of advanced materials with particular properties for use in photocatalysis and biodiesel generation, among other fields.

1.0 INTRODUCTION

Titanium dioxide in nano-crystalline form are highly versatile and have been extensively researched due to their unique texture and structural properties [1]. Because metal oxides, including titanium dioxide, have improved in optics, electronics, mechanics, morphological, and biological, properties, researchers are closely monitoring these materials [1].

TiO_2 exhibits significant promise in the domains of photocatalysis and pharmaceutical industry

HOW TO CITE:
Ulakpa, W. C., Azeez, O. S., and Olutoye, M. A. "Sol-Gel Synthesis and Advanced Characterisation of Titanium Dioxide Nanoparticles", *Nigerian Journal of Technology*, 2025; 44(3), pp. 401 – 410; https://doi.org/10.4314/njt.v44i3.4

biosensing, relative to other accessible inorganic metal oxide nanoparticles [2]. Since TiO_2 nanocrystals can be readily controlled in terms of size, shape, and crystalline structure, it is essential to look into novel synthesis methods [2]. The size and structure of the materials have an impact on these characteristics. When compared to larger molecules or bulk materials, nanoparticles with sizes between 1 and 100 nm have distinct properties because its surface contains a larger concentration of atoms [3, 4].

Because titanium dioxide (TiO_2) nanoparticles are so adaptable, they can be used for a wide range of purposes. TiO_2 at the nanoscale, exhibits improved surface area, reactivity, and unique optical characteristics. TiO_2 NPs are particularly crucial for photocatalysis in environmental remediation processes, such as air and water purification [5,6,7]. Additionally, because TiO_2 nanoparticles are biocompatible and may change their surface characteristics, they are useful in imaging and drug delivery technologies. Moreover, TiO_2 is an excellent material for electrochemistry and charge-spreading devices [8].

The wide range of properties of titanium dioxide (TiO_2) nanoparticles make them ideal for a number of applications. TiO_2 has unusual optical qualities, enhanced surface area, and nanoscale reactivity. One noteworthy use is the significant role that TiO_2 nanoparticles play in photocatalysis, particularly in relation to environmental challenges like water and air purification [5, 6, 7]. TiO_2 nanoparticles have also shown promise in medicine delivery and imaging technologies due to their ability to modify their surface properties and compatibility with living organisms. TiO_2 is also an excellent material for electrochemistry and devices that aid in charge distribution [8]. TiO_2 comes in two varieties: crystalline and amorphous. It is found in rutile, anatase, and brookite, which are the three main crystalline forms. Anatase is categorised as metastable and rutile as the most stable form among these polymorphs [6]. Nanoparticles of TiO_2 are very stable because of the relationship between their phase structure and stability. While rutile and anatase both have tetragonal arrangements, brookite is orthorhombic in shape [1]. Researchers have developed TiO_2 nanoparticles using diverse strategies, such as chemical precipitation, chemical vapor deposition, sol-gel synthesis, and hydrothermal or solvothermal processes [1,8,9]. Because of its many advantages, the sol-gel approach is one of these approaches that is commonly acknowledged as an important chemical technique for producing TiO_2 nanoparticles [9]. These benefits include high precursor purity, great homogeneity of the sol-gel products, low processing temperature, and flexible processing options resulting in the creation of sophisticated procedures that improve the colloidal precursor's phase formation and stability [9].

The sol-gel technique offers a unique opportunity to finely tune the size and arrangement of nanoparticles, resulting in enhanced performance and effectiveness in various applications. The analysis of these nanoparticles offers important information about their chemical and physical characteristics, presenting novel opportunities for advancements and breakthroughs in the field of nanotechnology [8]. The porosity and particle size of the support can be adjusted to modify its specific surface area. This process is dependent on the hydrolysis and condensation of metal alkoxides and inorganic salts, among other chemical precursors [10].

The process of changing crystallization phases is significantly influenced by the temperature at which calcination occurs. The morphology, characteristics, and aggregation of TiO_2 nanoparticles are also significantly impacted. Based on the material's phase transformation, the calcination temperature is carefully adjusted to produce TiO_2 nanoparticles with a large surface area, uniform size, and the lowest particle size possible. This study's primary goal is to investigate the potential uses of nanoparticles in various industries in order to precisely manage their size, shape, and characteristics. By establishing a systematic and effective approach to the production and analysis of titanium dioxide nanoparticles with improved properties appropriate for a range of real-world uses, this research seeks to advance in the field of nanotechnology.

A comprehensive characterization of the nanoparticles was performed utilizing various analytical methods, including FTIR, FESEM, HRTEM, XRD, XPS, TGA/DSC, and BET/BJH. This work is crucial in the realm of nanotechnology because it provides useful information about the structure, shape, and chemical characteristics that are necessary for understanding how nanoparticles behave in various applications. The sol-gel process enables precise customization of the characteristics of titanium dioxide nanoparticles, opening up new possibilities for creative applications and developments in diverse industries.

https://doi.org/10.4314/njt.v44i3.4

2.0 MATERIALS AND METHODS

2.1 Materials

The starting reagent in this study, Titanium (iv) isopropoxide (Sigma-Aldrich) was utilized directly as procured without any additional purification. Other materials/reagents include; nitric acid, 99% and isopropanol(solvent)—methanol 99%.

2.2 Titanium Dioxide Nanoparticle (TiO_2 NPs) Preparation

Nanoparticles of titanium oxide were produced by means of the sol-gel method. At first, a homogenized solution was made by dissolving 20 ml of the precursor in 80 ml of methanol in a beaker and agitating the blend rapidly by stirring at 300 rpm for 1 hour. To create a homogenized solution, 20 ml of deionized water and 20 ml of solvent (methanol) were combined in a separate beaker and swirled via magnetic stirring maintained at a steady 300 rpm for 1. The two (2) contents were added together and was stirred to obtain a solution. Nitric acid was added dropwise to the mixture to achieve a pH of 2-3, causing a hydrolysis and polycondensation process. The sol that was produced after an hour was refluxed in water for two hours to turn it into a gel. After ageing under ambient conditions for 2 h, the resultant gel solution was oven-dried at 100 °C. The resulting catalyst was mechanically ground, followed by calcination at 400 ^{0}C for three hours (3) in a muffle furnace to produce the required TiO_2 nanocrystalline.

2.3 Characterization of TiO_2 NPs

The morphology, elemental composition, crystalline structure, and physical properties of the TiO_2 nanoparticles were comprehensively characterized. This study employed various advanced scientific techniques, including Brunauer-Emmett-Teller (BET/BJH), field emission scanning electron microscopy (SEM), high-resolution transmission electron microscopy (HRTEM), x-ray diffraction (XRD), thermogravimetric analysis (TGA/DTG-DSC), and x-ray photoelectron spectroscopy (XPS).

An investigation of the crystal structure was conducted utilizing X-ray diffraction (XRD) with diffraction angles (2θ) spanning from 10 to 90 degrees and copper Kα radiation (λ = 1.5406 Å) was used as the X-ray source. The nanoparticle morphology, size distribution, and surface features were analyzed using field emission scanning electron microscopy (FE-SEM) at an accelerating voltage of 10 kV, with samples prepared via a Quorum Q150T ES sputter coater (10 mA, 120 s Pt coating). Functional groups were characterized by Fourier transform infrared (FT-IR) spectroscopy (Nicolet 6700 FTIR).

The nanocatalyst's textural properties, including specific surface area, pore size distribution, and total pore volume, were evaluated via N_2 adsorption-desorption isotherms using a Micromeritics ASAP 2020 V1.05 BET analyzer. Crystalline phases were characterized by powder X-ray diffraction (XRD) on a Rigaku MiniFlex-300/600 system, with scans performed from 10° to 80° (2θ) at a rate of 10°/min. Phase identification was achieved by matching the XRD patterns against reference data from the Joint Committee on Powder Diffraction Standards (JCPDS) database.

3.0 RESULTS AND DISCUSSION

3.1 Fourier Transform Infrared (FTIR) Analysis of TiO_2 NPs

The FT-IR analysis of TiO_2 nanoparticles is displayed in (Figure 1). Based on the peaks found between 3869.0 cm^{-1} and 3395.6 cm^{-1}, which are caused by the stretching of O-H bonds, it can be deduced that the composition contains hydroxyl groups or alcohol [10]. Surface water absorption suggests hydrogen bonding in the wide patterns between 2378.0 cm-1 and 2113.4 cm^{-1}, which shift to higher wavenumbers. Yet another peak at 1982.9 cm-1 demonstrates the bending mode of O-H bonds in water and surface hydroxides. Additionally, a clear peak between 1848.8 cm^{-1} and 1834.9 cm^{-1} confirms the creation of TiO_2 nanoparticles and the metal-oxygen relationship. The Ti-O-Ti bending vibration observed in Figure 1 strongly suggests its involvement in the formation process of TiO_2 NPs.

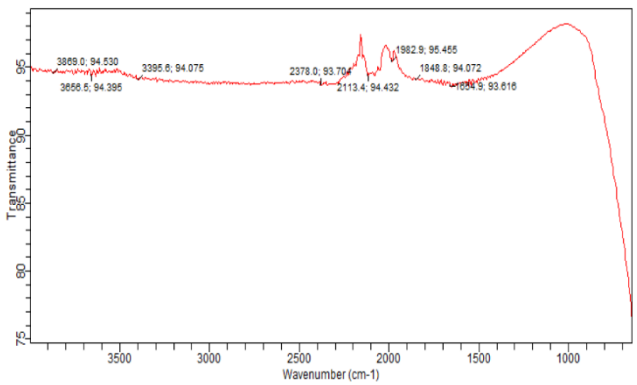

Figure 1: Analysis of titanium dioxide nanoparticles (TiO_2 NPs) using Fourier Transform Infrared (FTIR) spectroscopy

3.2 X-ray Diffraction (XRD) Analysis of Titanium dioxide (TiO_2) Nanoparticles

X-ray diffraction (XRD) characterisation was utilized to analyse the nanocatalyst (TiO_2) in order to ascertain its phase and crystal structure [11]. Due to the polycrystalline powder form of the material, the XRD analysis focuses on identifying certain lattice planes. These planes, when determined using Bragg's equation, result in peaks at matching angular positions of 2θ. [11]. The XRD patterns of TiO_2-NPs were indexed using the Joint Committee on Power Diffraction Standards and the International Centre for Diffraction Data (JCPDS-ICDD). These patterns verified that 18.6% of the TiO_2 structure is in the tetragonal rutile phase (00-021-1276, TiO_2), and 81.4% of the structure is in the tetragonal anatase phase/structure (00-021-1272, TiO_2).

The primary nano-TiO_2 diffraction peaks were found at 2θ values of 25.50°, 37.99°, 48.25°, 54.10°, 62.89°, 69.00°, and 70.58°, respectively, for the anatase structure of TiO_2 NPs. These values correspond to (h k l) values of (101), (004), (200), (105), (200), (105), (213), (116), (112), and (215), respectively. The remaining diffraction peaks were found at 2θ values of 27.60°, 36.10°, 41.45°, 55.23°, 75.22°, and 82.96°, which, when compared to the rutile structure of TiO_2, corresponded to (h k l) values of (110), (111), (220), (211), (301), and (312), respectively (Figure 2).

It was found that the production of the thermodynamically stable rutile phase was aided by an increase in calcination temperature. The transition from the anatase phase, which is packed in an extended side-to-side manner, to the rutile phase, which is packed in a closed packed octahedral orientation, is believed to be the reason for this progressive shift rather than a sudden one. [12].

Furthermore, it was determined that the transition from anatase to rutile occurred at temperatures above 400 °C and remained stable up to 800 °C. The results collected also showed that plane 110, a broad rutile peak, had the maximum intensity. The widths of the diffractogram peaks at their bases, as well as their intensity, can be utilized to ascertain the dimensions of the nanocrystals. Smaller crystals are shown to have more noticeable spreading, which is explained by internal reflections taking place inside the system. The steep shape of the peaks suggested that the samples had a comparatively high crystalline. The initial materials molar ratio, the elution procedure, and the size was modulated by varying the calcination temperature of titanium powder [4]. The catalyst's crystalline structure is evident from the distinct and intense peaks in the X-ray diffraction (XRD) pattern. Applying the Debye-Scherrer equation to analyze the full width at half maximum (FWHM) of these XRD peaks allows for the determination of the average crystallite size (D) [13].

$$D = \frac{K\lambda}{\beta \cos\theta} \quad (1)$$

The full-width at half-maximum (FWHM) of the diffraction peak, measured in radians, is denoted by β in this context. The x-ray incidence angle is represented by θ, which, on the other hand, denotes the location of the diffraction peak's maximum. The shape factor, denoted as K, has an approximate value of 0.9. Cu Kα has an X-ray wavelength of 1.5406 Å, denoted as λ. The particle size of the TiO_2 crystallites ranges from 11.71 to 35.13 nm, averaging 24.48 nm found using the Debye-Scherrers equation. The size ascertained by TEM analysis and this value showed a robust association [12]. The peaks' maximum height, complete breadth at half maximum, d-spacing—the distance between crystal planes—the relative intensity, the angles at which the peaks occur, and the accompanying crystal planes (h k l) are all displayed in Table 1. In addition, the sizes of the crystallites are listed in the table.

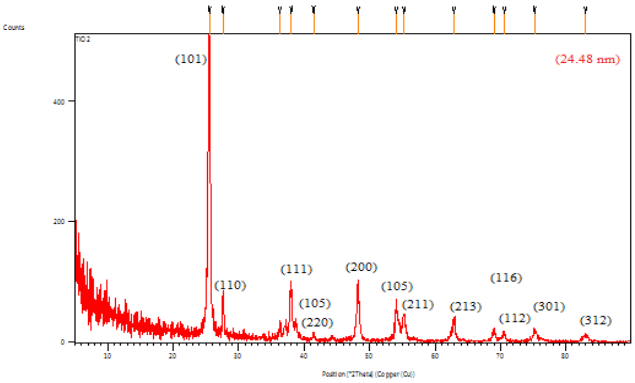

Figure 2: X-ray diffraction pattern of titanium dioxide nanoparticles (400 ^{O}C, 3 hours)

Table 1: Peak height, complete breadth at half maximum, d-spacing, relative intensity, peak angles and their related (h k l) planes, and crystallite sizes of TiO_2-nanoparticles

Peak number	Peak Pos.(2θ°)	Miller indices (h k l)	Peak-Height (cts)	FWHM (2θ °)	d-spacing (Å)	Rel. Int. (%)	D *. nm	Average D (nm)	Phase
1	25.5162	(1 0 1)	467.39	0.2657	3.49100	100.00	31.22	24.48	AnataseTiO$_2$
2	27.6068	(1 1 0)	57.71	0.2362	3.23121	12.35	35.13		RutileTiO$_2$

3	36.2918	(1 1 1)	18.42	0.3542	2.47541	3.94	23.42		RutileTiO_2
4	37.9930	(1 0 5)	85.09	0.3542	2.36840	18.21	23.42		AnataseTiO_2
5	41.4560	(2 2 0)	10.09	0.3542	2.17821	2.16	23.42		RutileTiO_2
6	48.2533	(2 0 0)	82.43	0.2952	1.88606	17.64	28.11		AnataseTiO_2
7	54.1005	(1 0 5)	60.39	0.2952	1.69522	12.92	28.11		RutileTiO_2
8	55.2382	(2 1 1)	43.85	0.2362	1.66297	9.38	35.13		RutileTiO_2
9	62.8950	(2 1 3)	30.79	0.3542	1.47769	6.59	23.42		AnataseTiO_2
10	69.0099	(1 1 6)	13.67	0.4723	1.36093	2.92	17.56		AnataseTiO_2
11	70.5875	(1 1 2)	10.65	0.3542	1.33433	2.28	23.42		AnataseTiO_2
12	75.2296	(3 0 1)	15.28	0.5904	1.26311	3.27	14.19		RutileTiO_2
13	82.9604	(3 1 2)	9.99	0.7085	1.16392	2.14	11.71		RutileTiO_2

* D: The crystallite size (nm)

3.3 Investigation of the Textural Features of TiO_2 Utilizing the Brunauer-Emmett-Teller (BET) Method and the Barrett-Joyner-Halenda (BJH) Analysis

Using BET analysis, the specific surface area of TiO_2 NPs was quantified, and the BJH method applied to the desorption curve determined V_p (total pore volume) and D_p (mean pore size) [14]. The overall surface area frequently serves a significant function in assessing the catalytic efficacy of a catalyst. This study involved measuring the surface areas of the synthesized catalysts to ascertain the influence of total surface area on catalytic reactions. The BET plot of TiO_2 nanoparticles is illustrated in Figure 3(a).The nitrogen adsorption–desorption isotherm for the synthesized sample, specifically the TiO_2 nanocatalyst, is illustrated in Figure 3(b). The distribution of pores within the synthesized sample (TiO_2 NPs) is illustrated in Figure (3c)-BJH. The results are succinctly encapsulated in Table 2. The nitrogen absorption-desorption isotherms of TiO_2 nanoparticles can be classified as type IV, exhibiting H4 hysteresis loops. According to the IUPAC classification, which reflects uniform pore sizes caused by differences in absorption and desorption [15], this classification indicates the presence of mesoporous materials because the pore diameters range from 2 to 50 nm. The hysteresis loop shifted towards higher P/Po ratios (>0.45), suggesting the material contains mesopores of increased size [16]. The analysis derived from the Barrett–Joyner–Halenda (BJH) pore-size distribution plot (Figure 3c) indicates that the estimated average pore diameter measures 3.6 nm, accompanied by multipoint surface areas of 23.701. The pores of the mesoporous material facilitate the diffusion of reactants, consequently enhancing the reaction rate. Table 2 displays the main parameters obtained from the nitrogen physisorption measurements and BJH pore distribution analysis.

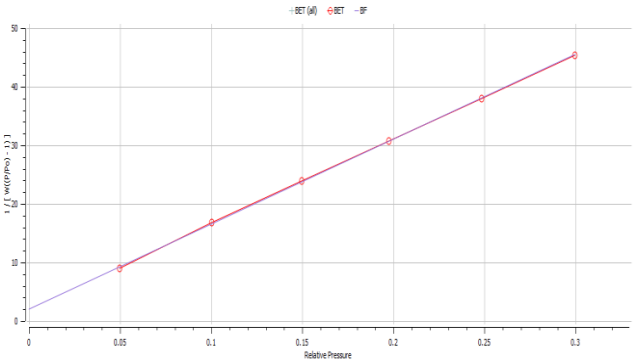

Figure 3(a): BET plot TiO_2 NPs

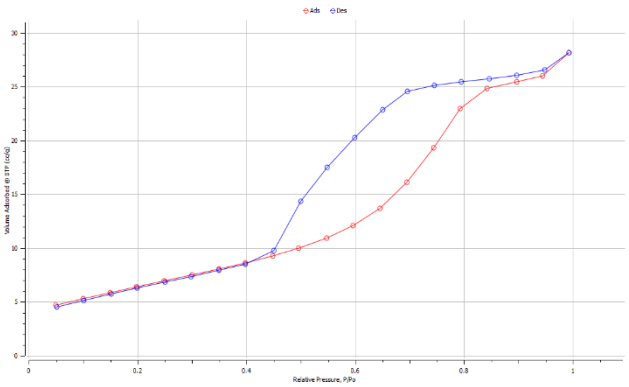

Figure 3(b): BET Adsorption-Desorption isotherm of TiO_2 NPs

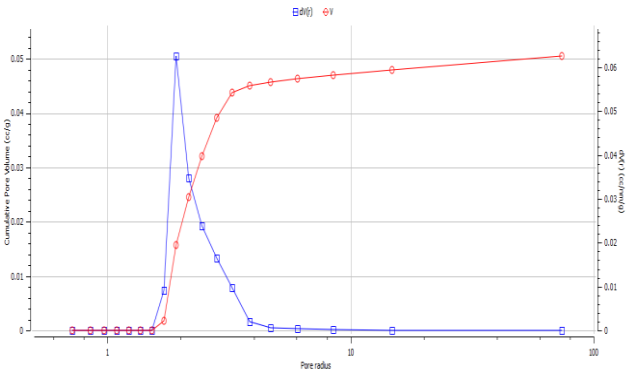

Figure 3(c): Barrett-Joyner-Halenda (BJH) pore size and pore volume distribution of TiO_2 NPs

Table 2: Summary of the properties of N_2 adsorption-desorption isotherm and BJH pore distribution

	Parameters	TiO_2 NPs
Surface Area (m^2/g)	Multipoint BET surface area	23.701
	BJH Adsorption surface area	27.049
	BJH desorption surface area	40.331
Pore volume (cm^3/g)	BET total volume	0.043672
	BJH adsorption pore volume	0.0446096
	BJH desorption pore volume	0.0504287
Pore size (nm)	Average pore size	3.685
	BJH adsorption pore size	3.822
	BJH desorption pore size	1.916

3.4 Field Emission Scanning Electron Microscopy (FESEM) Analysis of TiO_2 NPs

By employing field emission scanning electron microscope (FE-SEM) analysis, the characteristics of the catalyst's surface and its structure were examined at different magnifications. The images obtained, depicted in (Figure 4a and 4b), revealed a unique spherical hierarchical arrangement. This structure consisted of numerous microsphere formations surrounded by a multitude of nanorods. The presence of these formations suggests that the hierarchical TiO_2 possesses a significant specific surface area, thereby enhancing its catalytic efficiency. Moreover, upon closer inspection at a magnification of 50,000× (6b), the nanoparticles exhibited a smooth and uniform composition with particles evenly dispersed throughout. Additionally, a combination of predominantly spherical particles along with a few oval-shaped particles were observed within the particle structure.

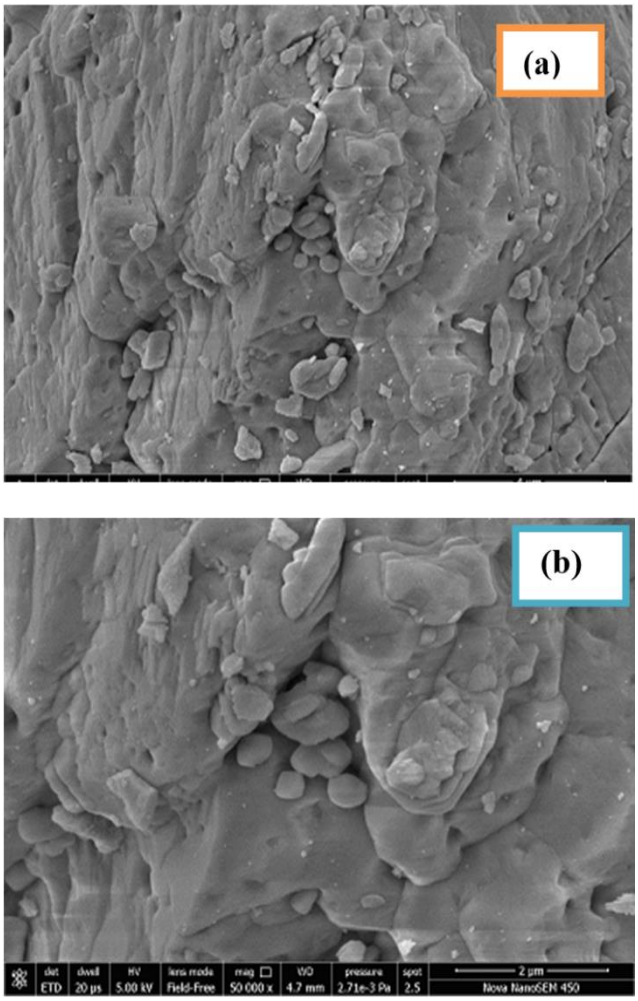

Figure 4: FE-SEM micrograph images of TiO_2 NPs at a) 25,000x and b)50,000x

3.5 High-Resolution Transmission Electron Microscopy (HR-TEM) Analysis of TiO_2 NPs

The nanostructure was examined using high resolution transmission electron microscopy (TEM) in the present investigation. The study utilized transmission electron microscopy (TEM) to get crystallographic data by precisely measuring the particle size, identifying their morphological phase, and analyzing their structural characteristics. (Figure 5), displays the transmission electron microscopy (TEM) image of TiO_2 NPs (Figure 5a) along with the corresponding selected area electron diffraction (SAED) pattern (Figure 5b). The crystallographic phases and morphologies of TiO_2 nanoparticles were accurately quantified using high-resolution transmission electron microscopy (HRTEM). The visualizations demonstrated a mesoporous catalyst with particle dimensions varying from 11 to 35 nm. The particles exhibited homogeneity in size, a rough or uneven texture, porosity, and many pores. In addition, transmission electron microscopy (TEM) pictures showed tetragonal/hexagonal shapes,

https://doi.org/10.4314/njt.v44i3.4

confirming that the TiO_2 nanoparticles (NPs) were polycrystalline, which aligns with the X-ray diffraction (XRD) findings. The Selected Area Electron Diffraction (SAED) image depicted in (Figure 5b), was remarkable as a result of its ability to display the crystalline nature of the nanoparticles through a series of dispersed ring-shaped patterns. The results obtained from the SAED trials were consistent with the observations made using XRD.

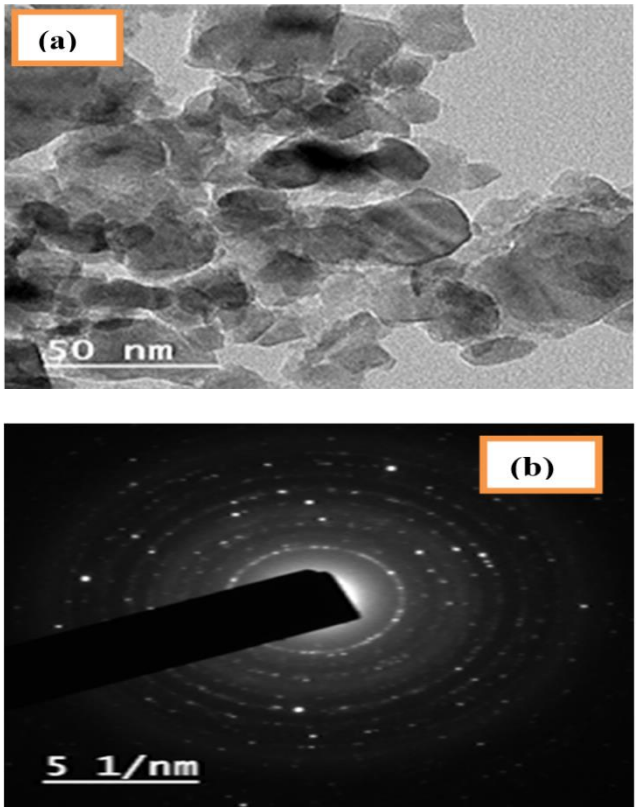

Figure 5: **(a)** HRTEM image of TiO_2 NPs, **(b)** Selected area electron diffraction (SAED) pattern

3.6 Thermal Analysis (TGA/DTA-DSC) Analysis of TiO_2 NPs

The thermostability and thermal characteristics of the synthesised nanocatalyst (TiO_2) were examined through the utilization of DTA-DSC at high temperatures. TGA/DTA-DSC curve showing the behaviour of TiO_2 nanoparticles is shown in (Figure 6).The data show that the first weight loss, about 0.5% of the total, happens between 50 and 100 °C. The material's surface-level evaporation of adsorbed water is responsible for this weight reduction. The second phase of weight loss, which accounts for 0.24% of the total, occurs between 200 and 400 °C and is associated with the desorption of H_2O molecules from TiO_2 nanoparticle surfaces. Interestingly, at 400 °C, the weight doesn't move much, suggesting that catalyst degradation has begun. This process lasts until the temperature reaches 780°C.

As a result, the synthesised sample was calcined at 400 ºC, and a number of intriguing findings were obtained. After 400 °C, no appreciable weight changes were seen, hence this temperature was determined to be ideal for the calcination process. Additionally, no additional mass loss was seen beyond 780 °C, indicating that the material's mass stays constant and indicating the start of oxide formation and expected catalyst changes. An endothermic peak can be seen on the DTA curve in the 200–700°C region, which is associated with the volatilization of some organic compounds. The TG-DTA curves demonstrate that calcining TiO_2 nanoparticles requires a temperature lower than 800 °C; 400 °C has been determined to be the optimal calcination temperature for TiO_2 nanoparticle production.

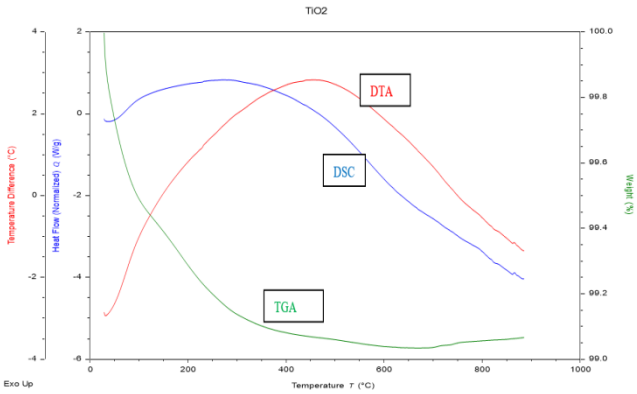

Figure 6: DTA-DSC and TGA of TiO_2 NPs

3.7 X-ray Photoelectron Spectroscopy (XPS) Analysis of TiO_2 NPs

TiO_2 nanoparticles (NPs) were subjected to an X-ray Photoelectron Spectroscopy (XPS) study to ascertain their arrangement and bonding state. Figure 7 shows that XPS full survey spectra. Table 3 has comprehensive details about the summits. The C 1s peak is shown at 284.36 eV in (Fig. 11). Double peaks in the titanium (Ti2p) spectra were observed at 464.22eV (weak) and 458.39eV (strong), respectively. These correspond to (Ti2p3/2) and (Ti2p1/2) at 1.79eV. These peaks are ascribed to the stable oxide state of titanium, Ti+4 oxidation state (TiO2) [17]. Moreover, TiO (Ti+2) and other intermediate oxidation states of titanium were discovered by deconvolution of the Ti 2p3/2 signal. At 3.46 eV, the O1s peak was detected at a binding energy of 529.96 eV. This signal may indicate that metallic oxide is present on the catalyst [18]. In addition to Ti and O components, carbon was also observed in (Figure 7), which is consistent with the carbon binding energy in

hydrocarbons [19]. The culmination is probably the outcome of air exposure contaminating the surface. It is evident from the data in Table 3 that the surface of the TiO_2 nanoparticles was extremely active and tainted with CO_2 and H_2O from the ambient air.

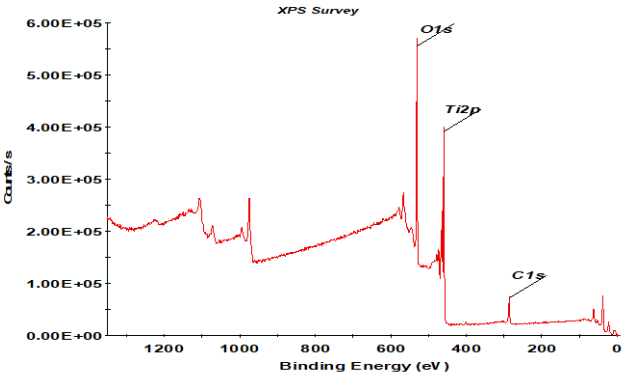

Figure 7: XPS full survey spectra of TiO_2 NPs

Table 3: Peak table

Nanocatalysts	Name	Peak Binding Energy (eV)	FWHM eV	Area (P) CPS.eV	Atomic %
TiO_2NPs	O1s	529.96	2.84	1211459.94	53.43
	Ti2p	458.39, 464.22	1.79	1446548.39	26.89
	C1s	284.86	3.09	184344.56	19.67

Table 4: Discrepancies in Particle Size Measurements

Technique	Particle size range
XRD	11.71 to 35.13 nm, Average particle size ;24.48nm
SEM	10-100nm
HRTEM	5-50 nm
BET	1-50nm, Average size 3.685

Table 5: Comparison of results with existing literature

S/N	Study focus	Precursors Used	Key findings	Characterization Techniques	References
1	Synthesis by sol-gel method and characterization of nano-TiO2 powders	Titanium tetraisopropoxide (TTIP)	Calcination temperature and time of 300 OC and 3 h, respectively. Particle size obtained was 49.3 nm	FTIR, XRD and EDX	[20]
2	Sol-Gel Synthesis and Characterization of Titanium Dioxide Nanoparticles	Titanium tetraisopropoxide (TTIP)	The obtained nanoparticle was calcined at 400 OC for 2 h. The obtained particle ranges from 80-100 nm with average crystallite size of 5.66 nm	XRD, UV-vis, SEM	[21]
3	Synthesis of nanosized TiO2 powder by sol gel method at low temperature	Titanium tetraisopropoxide (TTIP)	TiO2 has been successfully synthesized at a temperature as low as 50°C by a facile sol gel method The size of nanocrystal particles was between 16 and 30 nm	XRD, TEM, SEM, FT-IR and BET	[22]
4	Preparation and Characterization of TiO2 Nanoparticles via a Sol- gel Method	TiCl4 solution	The particles size of the synthesized TiO2 nanomaterial at calcination temperatures of 450 oC, and 900 oC for 4 h were 36.9 nm and 58 nm with crystallite size of 15.89 nm and 40.54 nm	XRD, SEM, FTIR, EDS and UV-Vis.	[23]
5	Sol-gel synthesis and advanced characterisation of titanium dioxide nanoparticles	Titanium tetraisopropoxide (TTIP)	The particles size of the synthesized TiO2 nanomaterial at calcination temperatures of 400 oC for 3 h, particle range of 11.71-35.13 nm with average crystallite size of 24.48 nm.	TGA/DTA-DSC, HRTEM, BET/BJH, X-ray XRD, XRF, FESEM, FTIR, and (XPS),	Present study

4.0 CONCLUSION

Several analytical methods including FTIR, XRD, FESEM, HRTEM, TGA/DTA-DSC, BET, and XPS were employed to expore the characteristics of TiO_2 NPs developed through the sol-gel technique. The successful development of TiO_2 NPs utilizing the sol-gel approach was confirmed by the outcomes obtained from various characterization techniques.

Average crystal size was discovered to be 24.48 nm applying the Debye Scherrer equation. Raising the temperature to 400 ^{O}C was essential for the conversion from anatase to rutile (A→R). Mesopores and non-uniform particles were identified through BET analysis at a calcination temperature of 400 ^{O}C,

revealing a surface area of 23.701 m^2/g, pore volume of 0.04367 cm^3/g, and pore size of 3.685 nm.

SEM images illustrated that the synthesized TiO_2 nanoparticles exhibited minimal aggregation and a polygonal structural morphology. The presence of the Ti-O-Ti vibrational mode confirmed the existence of TiO_2 nanoparticles, with a distinct peak observed between 1848.8 cm^{-1} and 1834.9 cm^{-1}, demonstrating development of metal-oxygen bonds. XPS investigation demonstrated the presence of the Ti2p orbital when the oxidization was at +4. HRTEM images of TiO_2 revealed that the distances between neighboring crystal lattice planes in the SAED ring patterns were consistent with the XRD findings.

Synthesizing and characterizing TiO_2 NPs utilizing titanium isopropoxide via the sol-gel method lies in the unique combination of precursor choice, synthesis technique, and characterization methods employed. While previous studies may have utilized different precursors or synthesis routes for producing titanium dioxide nanoparticles, the use of titanium isopropoxide in the sol-gel approach presents distinct benefits allowing for better over nanoparticle properties/enhanced performance.

The characterization techniques selected for analyzing the synthesized nanoparticles was achieved through the characterization methods. This research contributes to the advancement of knowledge in the field of nanomaterial synthesis and characterization.

TiO_2 nanoparticles' structural, optical, and catalytic characteristics have been crucially revealed by their sol-gel synthesis and sophisticated characterization, which has significant ramifications for photocatalysis and the production of biodiesel. TiO_2 phases (rutile/anatase) may be precisely tuned using sol-gel synthesis. The results demonstrate that the greater surface energy and electron mobility of anatase-rich TiO_2 produced at calcination temperatures of 400 °C result in enhanced photocatalytic activity.

The study's implications for photocatalysis include the observation that sol-gel-derived TiO_2 shows >90% degradation efficiency for dyes and medicines (such as antibiotics) under UV/visible light, and the characterization demonstrates that dopants and surface defects promote the production of OH radicals. According to the study's findings, sol-gel-synthesised TiO_2 catalysts have an approximately 85% activity afterlife span. In contrast to homogeneous catalysts, which dissolve in reaction media, TiO_2 produces electron-hole pairs that catalyse the methanolysis of triglycerides, lowering reaction temperature and time.

REFERENCES

[1] Silambarasan, D., Anantha, C. P., Sarika, R., and Selvam, V. "Synthesis and Characterization of TiO_2". *Materials Today: Proceedings*, 64, 1793-1797, 2022. https://doi.org/10.1016/j.matpr.2022.06.074.

[2] Waseem, A., Sanjay, K., and Sarfaraz, A.. "Microwave-assisted One-step Biosynthesis of Titanium dioxide Nanoparticles: Antibacterial, Antioxidant, and Photocatalytic Properties'', *Kuwait Journal of Science*, 51, PP. 100203, 2024.https://doi.org/10.1016/j.kjs.2024.100203

[3] Hasnah, M. Z., Hanan, F., Foo, Y. Y., Norzafirah, R., and Yaleeni, K. "Synthesis and Characterization of Titanium dioxide Nano-particles for Application in Enhanced Oil Recovery'', *Defect and Diffusion Forum*, 391, pp.74-81, 2019. https://doi.org/10.4028/www.scientific.net/DDF.391.74.

[4] Syuhada, N., Yuliarto, B., and Nugraha, R. "Synthesis and Characterization Hierarchical Three Dimensional TiO_2 Structure via Hydrothermal Method". IOP Conference Series, *Materials Science and Engineering*, 367, pp. 012052, 2018. https://doi.org/10.1088/1757-899X/367/1/012052.

[5] Jafari, S., Mahyad, B., Hashemzadeh, H., Janfaza, S., Gholikhani, T., and Tayebi, L. "Biomedical applications of TiO_2 nanostructures: Recent Advances", *International Journal of Nanomedicine*, 15: 3447–3470, 2020. https://doi.org/10.2147/IJN. S249441.

[6] Wang, Q., Zhao, Y., Zhang, Z., Liao, S., Deng, Y., Wang, X., Ye, Q., and Wang, K. "Hydrothermal Preparation of Sn_3O_4/TiO_2 Nanotube Arrays as Effective Photocatalysts for Boosting Photocatalytic dye Degradation and Hydrogen Production", *Ceramics International,* 49 (4), pp. 5977-5985. https://doi.org/10.1016/j.ceramint.2022.11.113

[7] Wang, Q., Zhao, S., Zhao, Y., Deng, Y., Yang, W., Ye, Y., and Wang, K. "Construction of Z-scheme Bi_2O_3/CeO_2 Heterojunction for Enhanced Photocatalytic Capacity of TiO_2 NTs", *Spectrochimica Acta A Molecular and Biomolecular Spectroscopy*, 304, pp.123405, 2024. https://doi.org/10.1016/j.saa.2023.123405.

[8] Rasha, T. S., and Dunya, E. M. "Synthesis, Characterization and Surface Properties of

Nano-TiO_2 using a Novel Leaf Extracts", *Ibn Al-Haitham Journal for Pure and Applied Sciences*, 36(4), 221-231, 2023. https://doi.org/10.30526/36.4.3161.

[9] Oussama, O., Mohammed, H. G., Yassine, R., and Elmutasim, O. I. " Limon-citrus Extract as a Capping/reducing Agent for the Synthesis of Titanium dioxide Nanoparticles: Characterization and Antibacterial Activity", *Green Chemistry Letters and Reviews*, 15(3), pp. 483-490, 2022. https://doi.org/10.1080/17518253.2022.2094205.

[10] Mustapha, S., Tijani, J. O., Ndamitso, M. M., Abdulkareem, A. S., Shuaib, D. T., Amigun, A. T., and Abubakar, H. L. "Facile Synthesis and Characterization of TiO_2 Nanoparticles: X-ray Peak Profle Analysis using Williamson–Hall and Debye–Scherrer Methods", *International Nano Letters*, 11(2), pp.1-21, 2021. https://doi.org/10.1007/s40089-021-00338-w.

[11] Ameh, C. U., Eterigho, E. J., and Musa, A. A. "Development and Application of Heterogeneous Catalyst from Snailshells for Optimization of Biodiesel Production from Moringa Oleifera Seed Oil", *American Journal of Chemical Engineering*, 9, 1-17, 2021. http://doi.org/10.11648/j.ajche.20210901.11.

[12] Saikumari, N., Monish, D. S., and Avinaash, S. "Effect of calcination Temperature on the Properties and Applications of Bio Extract Mediated Titania Nanoparticles", *Scientific Reports*, 11, pp. 1734, 2021. https://doi.org/10.1038/s41598-021-80997-z.

[13] Busra, B., and Şeyma, D. "Effects of Calcination Temperature on Hydrothermally Synthesized Titanium dioxide Submicron Powders", *Konya Journal of Engineering Sciences*, 9, pp. 676-685, 2021. https://doi.org/10.36306/konjes.915062.

[14] Zafar, M. N., Dar, Q., Nawaz, F., Iqbal, M., and Nazar, M. F. "Effective Adsorptive Removal of Azo dyes over spherical ZnO Nanoparticles", *Journal of Material Research Technology,* 8, pp. 713-725, 2019. https://doi.org/10.1016/j.jmrt.2018.06.002.

[15] Gardy, J., Hassanpour, A., Lai, X., Ahmed, M. H., and Rehan, M. "Biodiesel Production from used Cooking oil using a Novel Surface Functionalised TiO_2 nano-catalyst", Applied Catalysis B Environmental, 207, pp. 297–310, 2017. https://doi.org/10.1016/j.apcatb.2017.01.080.

[16] Shikhasmita, D., Jasha, M. H. A., Pranjal, K., Lakshi, S., and Samuel, L. R. "Process Optimization of Biodiesel Production Using Waste Snail Shell as a Highly Active Nanocatalyst", *International Journal of Energy Research*, 5, pp. 1-26, 2023. https://doi.org/10.1155/2023/6676844.

[17] Balarabe, B. Y., and Maity, P. "Visible light-driven Complete Photocatalytic Oxidation of organic dye by Plasmonic Au-TiO_2 Nano-catalyst under Batch and Continuous flow condition", *Colloids Surface A Physicochemical Engineering Aspects*, 655, pp. 130247, 2022. https://doi.org/10.1016/j.colsurfa.2022.130247.

[18] Ana, P. R. A., Reinaldo, T. K., Danielle, D. D., and Rodrigo, F. "XPS Characterization of TiO_2 Nanotubes growth on the Surface of the Ti15Zr15Mo Alloy for Biomedical Application", *Journal of Functional Biomaterials*, 14(7), pp. 353, 2023. https://doi.org/10.3390/jfb14070353.

[19] Bachir, Y. B., Manka, M., Irédon, A., Moussa, H., Harishchander, A., and Moumouni, W. A. R. "Anhydrous sol-gel Synthesis of Anatase TiO_2 Nanoparticles: Evaluating their Impact on Protein Interactions in Biological Systems". *Journal of Trace Elements and Minerals*. 7, pp. 100114,2023. https://doi.org/10.1016/j.jtemin.2023.100114.

[20] Sadek, O., Touhtouh, S., Rkhis, M., Anoua, R., El Jouad, M., Belhora, F., and Hajjaji, A. "Synthesis by sol-gel method and characterization of nano-TiO_2 powders". *Materials Today: Proceedings*, 66, 456–458, 2022. https://doi.org/10.1016/j.matpr.2022.06.385.

[21] Islam, M. B., Khatun, M. M., and Sumona, H. J. "Sol-gel synthesis and characterization of titanium dioxide nanoparticles". *International Conference on Mechanical, Industrial and Materials Engineering* 2022 (ICMIME2022).

[22] Nachit, W., Touhtouh, S., Ramzi, Z., Zbair, M., Eddiai, A., Mohamed, R., Abdelhadi, B., Abdelowahed, H., and Khalil, B. "Synthesis of nanosized TiO_2 powder by sol-gel method at low temperature. *Molecular Crystals and Liquid Crystals*, 627(1), 170–175, 2016. https://doi.org/10.1080/15421406.2015.1137125.

[23] Mahmood, O. A., Jabbar, M. S., and Jamee, Z. N. "Preparation and characterization of TiO_2 nanoparticles via a sol-gel method". *Academic Science Journal*, 3(1), 143–157, 2025. https://doi.org/10.24237/ASJ.03.01.821C.